Wideband Spectroscopy of Two Radio Bursts on AD Leonis

Rachel A. Osten[1]

T. S. Bastian

National Radio Astronomy Observatory, 520 Edgemont Road, Charlottesville, VA 22903
Electronic Mail: rosten@nrao.edu, tbastian@nrao.edu

ABSTRACT

We report high-time-resolution, broadband spectroscopic observations of two radio bursts on the classical flare star AD Leonis. The observations were acquired by the 305 m telescope at Arecibo Observatory on 2003 June 13-14. Using the Wideband Arecibo Pulsar Processor, these observations sampled a total bandwidth of 400 MHz, distributed over a 500 MHz frequency range, 1120–1620 MHz, with a frequency resolution of 0.78 MHz and a time resolution of 10 ms. A radio burst observed on June 13 is characterized by the presence of multitudes of short duration ($\Delta t \sim$30 ms), high brightness temperature ($T_b > 10^{14}$K), highly circularly polarized, fast-drift radio sub-bursts, with median bandwidths $\Delta\nu/\nu \sim$5%. The inverse drift rates are small, and have a symmetric distribution (both positive and negative frequency drifts) with a Gaussian FWHM inverse drift rate of 4.5×10^{-4} s/MHz. The fast-drift sub-bursts occur at a mean rate of 13 s^{-1} and show no evidence for periodic recurrence. The fast-drift radio events on AD Leo are highly reminiscent of solar decimetric spike bursts. We suggest the emission is due to fundamental plasma radiation. A second highly circularly polarized radio burst, recorded June 14, has markedly different properties: a smoothly varying intensity profile characterized by a slow drift in frequency with time (-52 MHz s^{-1}). Under the assumption that the source is due to a disturbance propagating through the low corona, a source size of 0.1–1 R$_\star$ is inferred, implying a brightness temperature range 6×10^{11}–6×10^{13}K: another example of a coherent radio burst.

Subject headings: stars: activity, stars: coronae, stars: late-type, radio continuum: stars

---

[1]Jansky Fellow, NRAO

1. Introduction

AD Leonis, a young disk star at a distance from the Sun of 4.9 pc, is one of the most active flare stars known. AD Leo produces intense, quasi-steady chromospheric and coronal emissions, with a 0.1–2.4 keV X-ray luminosity of 7×10^{28} erg s^{-1} (Hünsch et al. 1999), C IV λ 1548 luminosity of 9.5×10^{26} erg s^{-1} Hawley et al. (2003) and quiescent 20 cm radio luminosity of 5.5×10^{13} erg s^{-1} Hz^{-1} (Jackson et al. 1989). The star is also highly variable, producing flares at radio, optical, UV, EUV, and X-ray wavelengths (e.g., Bastian et al. 1990; Hawley & Pettersen 1991; Hawley et al. 2003, 1995; Favata et al. 2000).

Investigations of AD Leo's coronal characteristics led Güdel et al. (2003) to suggest that AD Leo is constantly undergoing small-scale coronal flare events, which explains the low-level variability as well as the intriguing plasma characteristics: namely, the high coronal electron densities of several $\times 10^{10}$ cm^{-3} and a concentration of plasma at temperatures 6–20 MK. Coronal densities and temperatures of this order are typically seen on the Sun during flares but not in quiescence. The distribution of flare frequency with energy on AD Leo is steep enough that flares may account for the entire observed X-ray luminosity, making the disparate nature of AD Leo's corona compared with the Sun's corona even more striking.

Radio bursts on AD Leo have been observed for many years, beginning with a report by Spangler et al. (1974). Radio bursts on AD Leo are characterized by large flux density enhancements – as large as ≈ 500 times the quiescent flux density level of ≈ 2 mJy – that can occur on very short time scales (< 0.02 seconds). The degree of circular polarization of the radio bursts is typically very high, often reaching 100% (Lang et al. 1983; Güdel et al. 1989; Bastian et al. 1990; Abada-Simon et al. 1997). The observations imply extremely large brightness temperatures during radio bursts, $T_b \geq 10^{15}$K, and suggest that one or more coherent radiation mechanisms operate in the corona of AD Leo. Both plasma radiation mechanisms and the cyclotron maser instability have been suggested as a means of accounting for the coherent radio emissions. Neither has been definitively ruled out by the observations.

Spectroscopic investigations of the coherent radio bursts on flare stars have typically been hampered by relatively long integration times (Bastian & Bookbinder 1987; Güdel et al. 1989) and/or limited bandwidths (e.g., Bastian et al. 1990; Abada-Simon et al. 1997). The necessary combination of high time resolution and broadband frequency coverage has only been available infrequently (Stepanov et al. 2001; Zaĭtsev et al. 2004), precluding the means to measure key parameters such as the intrinsic bandwidth of the radio bursts, thereby hampering their interpretation.

The recent upgrade of the Arecibo Observatory 305 m telescope has yielded a number of important improvements that motivated us to revisit the problem of coherent radio bursts on

AD Leo. First, the installation of a ground screen mitigates the problem of beam spillover, enabling users to track targets for longer periods of time with high sensitivity. Second, due to more complete illumination of the 305 m primary by the Gregorian feed (illumination area 213 m×237 m at zenith), the sensitivity of the telescope has improved. Finally, with the installation of Gregorian optics, a new broadband feed, and wideband receivers, the instantaneous bandwidth accessible has improved enormously. The relative bandwidth now accessible to Arecibo with the L-band wide receiver is $\Delta\nu/\nu = 36\%$, ten times the relative bandwidth previously available at Arecibo (Bastian et al. 1990), and more than three times the maximum relative bandwidths observed elsewhere (Stepanov et al. 2001; Zăıtsev et al. 2004). We therefore initiated a pilot program to observe dMe flares stars with the Arecibo 305 m telescope in June 2003, resulting in the detection of two radio bursts.

2. Observations

We observed AD Leo from 2003 June 12–15, during which time approximately 16 hours of data were collected. The observations were made using the "L-band wide" dual-linear feed and receiver, which provides frequency coverage from 1.15–1.73 GHz, with the Wideband Arecibo Pulsar Processor (WAPP) backend. The WAPP was selected because it provides the means of observing a large instantaneous bandwidth with excellent spectral and temporal resolution. The WAPP provides four data channels, each of 100 MHz bandwidth. These were deployed across the L-band wide receiver as follows: 1120–1220 MHz, 1320–1420 MHz, 1420–1520 MHz, and 1520–1620 MHz. A gap was deliberately left between 1220–1320 MHz to avoid the strong radio frequency interference (RFI) present in this frequency range. Nevertheless, the effects of other sources of RFI could not be entirely avoided in the frequency bands observed. We employed a data acquisition mode where data were sampled with a time resolution of 10 ms; 128 spectral channels were sampled across each 100 MHz channel, yielding a spectral resolution of 0.78 MHz. All four correlation products were recorded between the native-linear X and Y feed elements (XX, YY, XY, YX) with three-level sampling.

The beam size using the L-band wide receiver at 1.4 GHz is $\approx 3.1\times3.5$ arcminutes in azimuth and zenith angle. The 1σ noise uncertainty ranges from 28–43 mJy per frequency and time bin for the different WAPPs. Interferometric measurements of AD Leo's 1.4 GHz flux density during periods of apparent quiescence are ≈ 2 mJy (Jackson et al. 1989), well below the confusion limit of Arecibo at the observed frequencies (≈ 16–38 mJy from 1120 MHz to 1620 MHz). Our observing strategy was to observe the target, AD Leo, for 10 minute scans, and then to inject a correlated calibration signal to determine antenna temperatures. While there is a bright background radio source located ≈ 2.3 arcminutes away from AD Leo

(Seiradakis et al. 1995) and therefore within the primary beam, we utilized a "time-switching" scheme to difference times of burst activity ("on") and the quiescent state plus background ("off"). This procedure enabled us to estimate the antenna temperature and flux density through the use of gain curves as a function of azimuth and zenith angle.

3. Data Analysis and Results

Two radio bursts were identified in the WAPP data. The first radio burst occurred from approximately 22:35:20–23:36:30 UT on 2003 June 13 and the second occurred from approximately 20:05:40–20:06:30 UT on 2003 June 14. We now describe the observations, their analysis, and results for each event in turn.

3.1. Event on June 13

Figure 1 displays the dynamic spectrum of the event June 13 in both the Stokes I (total flux) and V (circularly polarized flux) parameters. The radio burst is characterized by the following general properties:

- The burst duration is a few 10s of seconds.

- The peak flux is ≈ 200 mJy.

- The flux is strongly modulated in time, showing discrete features that have rise times of ≈ 20 ms.

- The radio burst displays clear substructure in the time-frequency domain.

- The radio sub-bursts are highly circularly polarized ($> 90\%$).

In these respects, the properties of this radio burst are quite similar to those of strong radio bursts reported previously (Lang et al. 1983; Güdel et al. 1989; Bastian et al. 1990; Abada-Simon et al. 1997) in this frequency band. Indeed, noting the fast rise times of discrete sub-bursts, a light travel time argument implies source sizes $l \approx c\Delta t \sim 9 \times 10^8$ cm, or 4% of the stellar radius, $R_\star$. Using this scale as an estimate of the source size ($R_s < 6000$ km), the observed bursts are consistent with brightness temperatures $T_B > 4 \times 10^{14}$ K. Such large brightness temperatures in AD Leo's corona require a coherent emission process.

Given the greatly increased bandwidth of these observations, a number of new properties of coherent radio bursts on AD Leo can be identified and analyzed. In particular, multitudes of time-resolved and spectrally-resolved structures are present in the spectrum (see Figures 2 and 3). We note that the presence of this fine structure is incompatible with diffractive scintillation resulting from propagation of the signal from AD Leo to the telescope. The bandwidth and time scale characteristic of scintillation are expected to be of order several GHz and $\sim 10^6$ sec, respectively. We therefore believe the observed fine structure is intrinsic to the source. We refer to these fine structures as "sub-bursts". The start frequency, duration, bandwidth, and drift rate of individual sub-bursts can be characterized, offering new constraints on the emission mechanism responsible for the observed emission.

3.1.1. Methodology

In order to characterize quantitatively the multitudes of fast-drift radio sub-bursts that comprise this event, we employ an algorithm based on Aschwanden & Benz (1986), originally used to analyze solar radio bursts at decimeter wavelengths. We note that the discrete radio sub-bursts observed on AD Leo are well-resolved in frequency. Therefore, the dynamic spectrum was binned over 4 adjacent frequency channels to improve the signal to noise ratio without loss of spectral information. Threshold fluxes were calculated using rms flux values from "off" times for each WAPP data channel; a 3σ flux density threshold of ≈ 45 mJy was applied using the binned dynamic spectrum. Then, first and second derivatives are computed, and times when the conditions

$$\partial S_{ij}/\partial t_i > 0, \tag{1}$$

$$\partial^2 S_{ij}/\partial t_i^2 < 0, \tag{2}$$

$$\partial S_{i+1,j}/\partial t_{i+1} < 0 \tag{3}$$

where S_{ij} is the flux density at time i and frequency channel j, were used to identify peaks in each channel. The time, frequency, and flux density of each pixel which satisfied the above conditions were recorded. Individual sub-bursts were identified using an algorithm to group peaks across channels. This is an IDL procedure adapted from a photometry routine in the IDL Astronomy User's Library[1] to group stars with non-overlapping PSF profiles into distinct groups. Instead of using (x,y) as distances, the data points are (time,frequency) and the distances of any given point from any other point in time and frequency are calculated

---

[1] Available at http://idlastro.gsfc.nasa.gov/contents.html.

separately. The critical grouping describes the distances in time and frequency within which the peaks must lie to be in the same group. We explored the probability space of these critical grouping time and frequency values, to determine those values in which the probability of having $> n$ peaks occurring at random was sufficiently low, $\leq 10^{-5}$, and found that requiring n to be 5 and restricting $t_{\mathrm{crit}} \leq 20$ ms, $\nu_{\mathrm{crit}} \leq 20$ MHz was sufficient to meet this condition. Using this procedure, we identified 313 individual sub-bursts.

Inverse drift rate, start frequency, duration, and bandwidth for the sub-bursts were then determined. We filtered the data for bursts which appeared to continue beyond our frequency limits, and required that the flux spectrum of the burst at a given time was Gaussian-like, estimating the bandwidth from the FWHM of a third degree polynomial fit to the flux spectrum (Csillaghy & Benz 1993). The burst duration was calculated as the median FWHM of a parabolic fit to the temporal variations of all frequency channels in which peaks were identified. The start frequencies and inverse drift rates were calculated for sub-bursts which had more than one unique time peak. Out of 313 discrete events identified by the above procedure, we determined bandwidth and duration for 180 sub-bursts, and inverse drift rate and start frequencies for 121 sub-bursts. Figure 4 displays the distributions of these four quantities.

3.1.2.   Rates and Durations

The median sub-burst duration is 0.03 seconds. The average sub-burst rate is 13 per second during the time when bursting activity is evident, with a maximum of ≈ 45 s^{-1}. Light curves of the bursting behavior in two different bands are illustrated in Figures 2 and 3. A power spectrum analysis of light curves reveals no evidence for periodicities in the data, although previously reported bursts do show quasi-periodic oscillations in some cases (Lang & Willson 1986; Bastian et al. 1990; Güdel et al. 1989; Stepanov et al. 2001).

3.1.3.   Start Frequencies and Bandwidths

The bursts are confined to frequencies above 1350 MHz, reaching a peak just below a frequency of 1500 MHz. Figure 2 shows that the sub-bursts appear to be fast-drift structures. Some structures drift to higher frequencies with time, while others drift to lower frequencies with time.

Figure 4 details the distribution of bandwidths. The median fractional bandwidth is 5%, with individual bursts having measured bandwidths up to 15%. The minimum and

maximum bandwidths we are able to determine with our data are $\Delta\nu/\nu$=1% and 36%, respectively.

3.1.4. Inverse Drift Rates

Figure 4 displays the inverse drift rate distribution for events with nonzero duration; the observed distribution is symmetric. The absolute value of the smallest inverse drift rates measurable with our data set arise from a combination of the minimum duration and maximum bandwidth, 0.01 s and 487 MHz, respectively, or 2×10^{-5} s MHz^{-1}. A Gaussian fit to the distribution, illustrated in Figure 4 has a FWHM of 4.5×10^{-4} s MHz^{-1}, corresponding to a characteristic drift rate of 2.2 GHz s^{-1}. The distribution of inverse drift rates is incompatible with interstellar dispersion, which would be expected to have a value $\approx -1.5 \times 10^{-6}$ s MHz^{-1} for the dispersion measure of AD Leo ($\sim$0.5 pc cm^{-3}) at these frequencies (Rybicki & Lightman 1979).

3.2. Event on June 14

The dynamic spectrum of the event on June 14 in Stokes I and V is displayed in Figure 5. While similar in duration to the June 13 event, it otherwise differs significantly from it. The June 14 emission is characterized by a smooth variation with time rather than the spiky emission seen on June 13. By eye the event appears to contain sub-structure, and we explored the possible existence of quasi-periodic oscillations in the data. Although there were peaks in the periodograms at 0.5 and 40 Hz for each rebinned channel, these periods appeared in the data directly preceding and following the event as well, casting doubt on the reality of finer temporal scale structures in the event.

Light curves (Figure 6) show that the time variation of the emission has an approximately Gaussian variation. Both the duration of the emission and the time of peak flux evolve towards lower frequencies. The data were averaged in frequency by a factor of 10 and in time by a factor of 20 to ameliorate the statistics, and were then fit to a Gaussian time profile in each frequency bin. Figure 7 displays the variation of the Gaussian parameters (center, width, peak). The peak times of the Gaussians drift with frequency at a rate of -52 MHz/s from 1120–1490 MHz, a drift rate that is far smaller than those characteristic of the sub-bursts observed on June 13. The event apparently extends to both lower and higher frequencies. The lower limit on the bandwidth of the emission is therefore $\Delta\nu/\nu > 36\%$. The duration of the event decreases with frequency. As was the case for the June 13 event,

the degree of circular polarization is high ($> 50\%$), but less well constrained than the June 13 event as a result of the poorer signal to noise ratio.

The lack of temporal and spectral fine structures prevents us from using such features to constrain the source size. Presuming the source is comparable in scale to the star itself ($l_S \approx R_\star \approx 0.5R_\odot$), a brightness temperature of $\approx 2 \times 10^{11}$ K is obtained. This might suggest that an incoherent emission mechanism (e.g., synchrotron radiation) is feasible. However, the high degree of circular polarization indicates otherwise. We conclude that, like the June 13 event, the June 14 event is likely due to a coherent emission mechanism. If so, the source scale l_S may be considerably smaller than the size of the star: $l_S \approx 5 \times 10^{10}\mathrm{T}_{\mathrm{B10}}^{-1/2}$ cm, where $\mathrm{T}_{\mathrm{B10}}$ is the brightness temperature in units of 10^{10} K.

4. Discussion

We have concluded that, given the extremely high brightness temperatures and the high degree of circular polarization observed, a coherent emission mechanism or mechanisms is/are responsible for the radio bursts observed on AD Leo on 2003 June 13 and 14. We now discuss each event in turn.

4.1. June 13 Event

It is useful to draw parallels between the properties of the June 13 radio burst observed on AD Leo and radio bursts observed in the solar corona, recognizing that such parallels must not be given undue emphasis. A summary of different types of solar radio bursts is given in Table 1 of Dulk (1985). More recently, work on decimeter- wavelength and microwave solar bursts has been summarized by Bastian et al. (1998). A striking feature of the June 13 event is the presence of multitudes of fast drift sub-bursts. This might suggest that a phenomenon analogous to solar decimetric type III bursts (type IIIdm) or solar spike bursts may be relevant.

Like meter wavelength type III radio bursts, type IIIdm bursts are fast-drift bursts that occur as a result of the nonlinear conversion of plasma waves (Langmuir waves) to electromagnetic radiation at the local electron plasma frequency $\nu_{pe} = \sqrt{e^2 n_e / \pi m_e} \approx 9 n_e^{1/2}$ kHz or its harmonic $2\nu_{pe}$. The Langmuir waves are believed to be excited by the passage of a suprathermal electron beam propagating at a speed of $\sim 0.1 - 0.3c$. If the beam propagates from lower (denser) to greater (more rarefied) heights in the corona, the radio emission drifts from high to low frequencies. If the beam propagates from greater to lower heights,

the radio emission drifts with time in the opposite sense. In some respects, type IIIdm may be regarded as the high frequency extension of classical type III radio bursts. However, for metric type III bursts the vast majority drift from high to low frequencies, indicating a beam exciter that propagates from high to low densities in the corona. The same is not true for type IIIdm bursts. In particular, the majority of type IIIdm bursts drift with frequency in the opposite sense to that of metric type IIIs, indicating most are due to electron beams propagating from lower to higher densities.

Closer examination of the properties of the sub-bursts determined in §3.1 suggests that the June 13 event bears closer resemblance to solar decimetric spike bursts. Decimetric spike bursts have generated interest since their discovery (Dröge 1977) as phenomena possibly closely linked with magnetic energy release in the solar corona (Benz 1986). They differ from type III dm bursts in several critical respects. First, their instantaneous bandwidths typically are an order of magnitude less than those of type IIIdm bursts. Second, their durations are also roughly an order of magnitude smaller than those of type IIIdm bursts. Indeed, the decay times of the decimeter spike bursts may be consistent with electron-ion collisional damping (Güdel & Benz 1990), unlike those of type III and type IIIdm bursts. Third, again in contrast to type IIIdm bursts, the degree of circular polarization of spike bursts tends to be high, at least for those observed on the disk of the Sun where propagation effects are expected to be small (Güdel & Zlobec 1991). Unlike type III or type IIIdm bursts, the distribution of frequency drifts shows no strong preference for predominantly positive or negative drifts. A study by Güdel & Benz (1990) demonstrated that the distribution of *inverse* drift rates of solar decimetric spikes is roughly symmetric at 362 and 770 MHz. These were interpreted as a nearly isotropic distribution of exciter directions within the context of plasma radiation.

To a striking degree, the June 13 event is similar in its properties to solar decimetric spike bursts, an exception possibly being the durations of the discrete bursts, which appear to be a few times longer than solar spike bursts at the same frequency, a point to which we return below. While plasma radiation produced by the nonlinear conversion of Langmuir waves excited by the passage of an electron beam is the accepted emission mechanism for type III and type IIIdm bursts on the Sun, the emission mechanism for decimetric spike bursts is more controversial. One possibility is the electron cyclotron maser (ECM) mechanism, which operates at the fundamental or harmonic of the local electron gyrofrequency $\Omega_{Be} = eB/2\pi mc = 2.8B$ MHz when $0.3 < \omega_{pe}/\Omega_{Be} < 1$ (see, e.g., Fleishman & Melnikov 1998, for a review). The other possibility is a plasma radiation process. Neither mechanism has been shown unambiguously to be the mechanism responsible for solar decimetric spike bursts. Likewise, neither mechanism can be firmly identified as that responsible for the spike bursts on AD Leo although, for reasons we now outline, a plasma radiation mechanism is favored.

The primary reason we favor plasma radiation over the ECM is that in the hot, dense corona of AD Leo, radiation generated by the ECM at the first or second harmonic of Ω_{Be} can be readily gyroresonantly absorbed at the second or third harmonic layers, respectively. Although the situation may be avoided or mitigated (see Fleishman & Melnikov 1998, and references therein) in the solar corona, the problem is exacerbated in the corona of AD Leo, which is significantly hotter than the Sun's. Whereas the bulk of solar X-ray-emitting thermal plasma in quiescence is 1–2 MK, AD Leo's corona is dominated by 6–20 MK soft X-ray-emitting plasma. Since the gyroresonance absorption coefficient increases as $\kappa_{gr} \sim T^{s-1}$, where $s = 2, 3$ is the harmonic of the absorbing layer, the absorption is significantly greater in the corona of AD Leo than it is in the Sun's corona. In contrast to ECM radiation, plasma radiation is most susceptible to free-free absorption. Unlike gyroresonance absorption, however, the efficacy of free-free absorption decreases with increasing plasma temperature as $\kappa_{ff} \propto T^{-3/2}$. Hence, the higher temperature of AD Leo's corona favors the escape of radiation generated via a plasma radiation mechanism over that generated by the ECM mechanism if $\omega_{pe} > \Omega_{Be}$. For fundamental plasma radiation, this suggests $B < 500$ G, a condition easily and widely met in the corona of AD Leo. Moreover, Zaĭtsev et al. (2000) have argued that plasma radiation mechanisms operate significantly more efficiently in the hot corona of late-type stars.

Assuming, therefore, that the burst emission on AD Leo is due to fundamental plasma radiation, the symmetry of the inverse drift rate distribution implies an isotropic distribution of exciters with respect to the electron density gradients. If a given exciter is a beam propagating through AD Leo's corona, the drift rates imply (e.g., Benz 2002)

$$\frac{d\nu}{dt} = \frac{\partial \nu}{\partial n_e} \frac{\partial n_e}{\partial h} \cos\phi \frac{\partial s}{\partial t}, \tag{4}$$

where n_e is the ambient electron density, h is the vertical height, $\partial h = \partial s \cos\phi$, $\cos\phi$ is the angle between the beam direction and the vertical, and $\partial s/\partial t = v$ is the propagation speed. Approximating the density variation as an exponential with a scale height H_n, this equation can be rewritten $\dot{\nu} \sim -(\nu v \cos\phi)/(2H_n)$ and so $v \sim -2H_n\dot{\nu}/\nu \cos\phi$. Taking the FWHM inverse drift rate of 4.5×10^{-4} s MHz^{-1}, $\dot{\nu} = 2.2$ GHz s^{-1}, $v \sim 4H_n$ for $\phi \approx 45$ degrees. Constraining v to be $0.1c - 0.5c$ suggests a scale height of order $1 - 4 \times 10^9$ cm. The isothermal scale height for a 10 MK plasma around a star of mass $\sim$0.3 M$_\odot$ and radius $\sim$0.3R$_\odot$ is about a factor of ten larger than this scale height, suggesting that the scale height deduced from the drift rate may indicate an inhomogeneity size scale in AD Leo's corona within which the sub-burst exciters are propagating. Interestingly, if we constrain the event duration ($\tau \sim$0.03 s) to be of order the Coulomb deflection time, the temperature in the source can in turn be constrained:

$$T \sim 8000\nu_6^{4/3}\tau^{2/3} \approx 13\text{MK} \tag{5}$$

where ν_6 is the observed frequency in MHz. This value is comparable with coronal temperatures inferred from SXR observations.

4.2. Event of June 14

The second event is markedly different from the June 13 event. It is characterized by a smoothly varying continuum in time and frequency. As shown in §3.2, the time variation of the emission at a given frequency is well-approximated by a Gaussian profile. The Gaussian width and the time of maximum progressively increase with decreasing frequency. In contrast to the fast-drift bursts in the June 13 event, which had characteristic drift rates of 2.2 GHz s^{-1}, the drift rate of the June 14 event is -52 MHz s^{-1}. The drift of the event could be due to a disturbance propagating through AD Leo's corona. Under this interpretation, the observed drift rate value of -52 MHz s^{-1} implies that the disturbance is propagating outward; taking $\nu = 1490$ MHz for the approximate starting frequency, at coronal temperatures $(T = 10^6, 10^7\text{K})$, the observables constrain the propagation speed to be $(1200, 1.2\times10^4)$ km s^{-1}, assuming that it is fundamental plasma emission. Associating the observed frequencies with fundamental plasma emission produces a constraint on the ambient electron density, $n_e \leq 3\times10^{10}$ cm^{-3}, which is consistent with measurements of cool SXR-emitting coronal material ($n_e \leq 3\times10^{10}$ cm^{-3} at T$\sim$2MK; van den Besselaar et al. 2003). These speeds are consistent with the Alfvén speed in a medium with $B \leq 100$ (1000) G, $n_e \leq 3 \times 10^{10}$ cm^{-3} for 1200 (1.2×10^4) km s^{-1}, respectively. The maximum duration (FWHM) is $\sim$23s, which implies that the extent of the atmosphere through which the disturbance propagated is 0.1 (1) R$_\star$, for $v =$1200 (1.2×10^4) km s^{-1}, respectively. Such a source size, coupled with the estimates of the maximum flux density, constrain the brightness temperature to be 6×10^{11}–6×10^{13}K.

5. Summary and Conclusions

We have presented wideband dynamic spectra of two radio bursts observed on the dMe flare star AD Leo. The observed properties of the two bursts indicate that a coherent emission mechanism is responsible. A plasma radiation mechanism is favored. The first event, on 2003 June 13, contained multitudes of fast-drift bursts that were similar in their properties to solar decimetric spike bursts. In particular, the distribution of their bandwidths, inverse drift rates, and the high degree of circular polarization were qualitatively and quantitatively

similar to solar spike bursts. The distribution of durations were a factor of ~ 3 greater than their solar analogs. The observations are consistent with the idea that the spike bursts are due to fundamental plasma radiation driven by electron beam exciters. The burst durations are consistent with the collisional decay time. We attribute the fact that they are longer-lived than their solar analogs to the greater temperature of the coronal medium on AD Leo. The second event, on 2003 June 14, was different in character from the first event, being characterized by a smoothly varying continuum and frequency drift rate significantly smaller than the fast-drift bursts on June 13. The emission mechanism responsible for the burst is less certain, but if it is plasma radiation, the observed drift rate is consistent with a disturbance propagating in the stellar corona with a speed comparable to the local Alfvén speed.

We conclude by pointing out that the upgrades to the Arecibo Observatory and the Green Bank Telescope now open up wide regions of frequency space which can be observed simultaneously at high time resolution. These advances in technology allow for dynamic spectrum analysis of bursting phenomena on stars using techniques used for decades on the Sun. Such instrumental advances allow an investigation of plasma physics in stellar environments on the smallest spatial and temporal scales yet obtained. These investigations are crucial to establishing the extent to which solar phenomena can be applied in extreme stellar environments.

REFERENCES

Abada-Simon, M., Lecacheux, A., Aubier, M., & Bookbinder, J. A. 1997, A&A, 321, 841

Aschwanden, M. J. & Benz, A. O. 1986, A&A, 158, 102

Bastian, T. S., Benz, A. O., & Gary, D. E. 1998, ARA&A, 36, 131

Bastian, T. S., Bookbinder, J., Dulk, G. A., & Davis, M. 1990, ApJ, 353, 265

Bastian, T. S. & Bookbinder, J. A. 1987, Nature, 326, 678

Benz, A. 2002, Plasma Astrophysics, Kinetic Processes in Solar and Stellar Coronae, second edition (Astrophysics and Space Science Library, Vol. 279, Kluwer Academic Publishers, Dordrecht, 2002.)

Benz, A. O. 1986, Sol. Phys., 104, 99

Csillaghy, A. & Benz, A. O. 1993, A&A, 274, 487

Dröge, F. 1977, A&A, 57, 285

Dulk, G. A. 1985, ARA&A, 23, 169

Favata, F., Micela, G., & Reale, F. 2000, A&A, 354, 1021

Fleishman, G. D. & Melnikov, V. F. 1998, Phys.-Uspekhi, 41, 1157

Güdel, M., Audard, M., Kashyap, V. L., Drake, J. J., & Guinan, E. F. 2003, ApJ, 582, 423

Güdel, M. & Benz, A. O. 1990, A&A, 231, 202

Güdel, M., Benz, A. O., Bastian, T. S., Furst, E., Simnett, G. M., & Davis, R. J. 1989, A&A, 220, L5

Güdel, M. & Zlobec, P. 1991, A&A, 245, 299

Hünsch, M., Schmitt, J. H. M. M., Sterzik, M. F., & Voges, W. 1999, A&AS, 135, 319

Hawley, S. L., Allred, J. C., Johns-Krull, C. M., Fisher, G. H., Abbett, W. P., Alekseev, I., Avgoloupis, S. I., Deustua, S. E., Gunn, A., Seiradakis, J. H., Sirk, M. M., & Valenti, J. A. 2003, ApJ, 597, 535

Hawley, S. L., Fisher, G. H., Simon, T., Cully, S. L., Deustua, S. E., Jablonski, M., Johns-Krull, C. M., Pettersen, B. R., Smith, V., Spiesman, W. J., & Valenti, J. 1995, ApJ, 453, 464

Hawley, S. L. & Pettersen, B. R. 1991, ApJ, 378, 725

Jackson, P. D., Kundu, M. R., & White, S. M. 1989, A&A, 210, 284

Lang, K. R., Bookbinder, J., Golub, L., & Davis, M. M. 1983, ApJ, 272, L15

Lang, K. R. & Willson, R. F. 1986, ApJ, 305, 363

Rybicki, G. B. & Lightman, A. P. 1979, Radiative processes in astrophysics (New York, Wiley-Interscience, 1979. 393 p.)

Seiradakis, J. H., Avgoloupis, S., Mavridis, L. N., Varvoglis, P., & Fuerst, E. 1995, A&A, 295, 123

Spangler, S. R., Rankin, J. M., & Shawhan, S. D. 1974, ApJ, 194, L43

Stepanov, A. V., Kliem, B., Zaitsev, V. V., Fürst, E., Jessner, A., Krüger, A., Hildebrandt, J., & Schmitt, J. H. M. M. 2001, A&A, 374, 1072

van den Besselaar, E. J. M. and Raassen, A. J. J. and Mewe, R. and van der Meer, R. L. J. and Güdel, M. and Audard, M. 2003, A&A, 411, 587

Zaĭtsev, V. V., Kislyakov, A. G., Stepanov, A. V., Kliem, B., & Furst, E. 2004, Astronomy Letters, 30, 319

Zaĭtsev, V. V., Kupriyanova, E. G., & Stepanov, A. V. 2000, Astronomy Letters, 26, 736
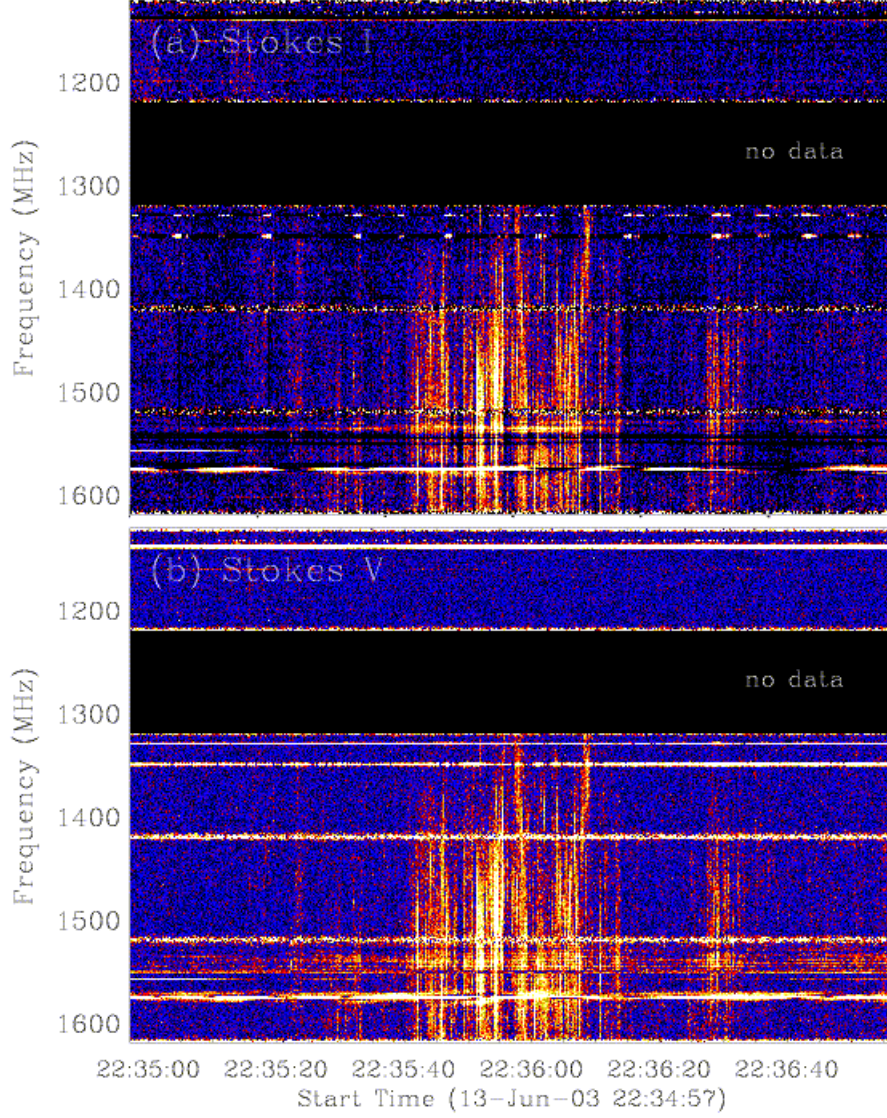
Fig. 1.— Dynamic spectrum of fast drifting behavior seen on AD Leo with the Arecibo Observatory. Frequency increases down and time increases to the right. Frequency coverage extends from 1120–1220 MHz, 1320–1620 MHz; gaps are due to RFI excision or poor bandpass response. The data have been rebinned by a factor of 4 in frequency, and are illustrated at the full time time resolution of 0.01s. *(a)* Dynamic spectrum of total intensity variations. *(b)* Dynamic spectrum of circular polarization variations.
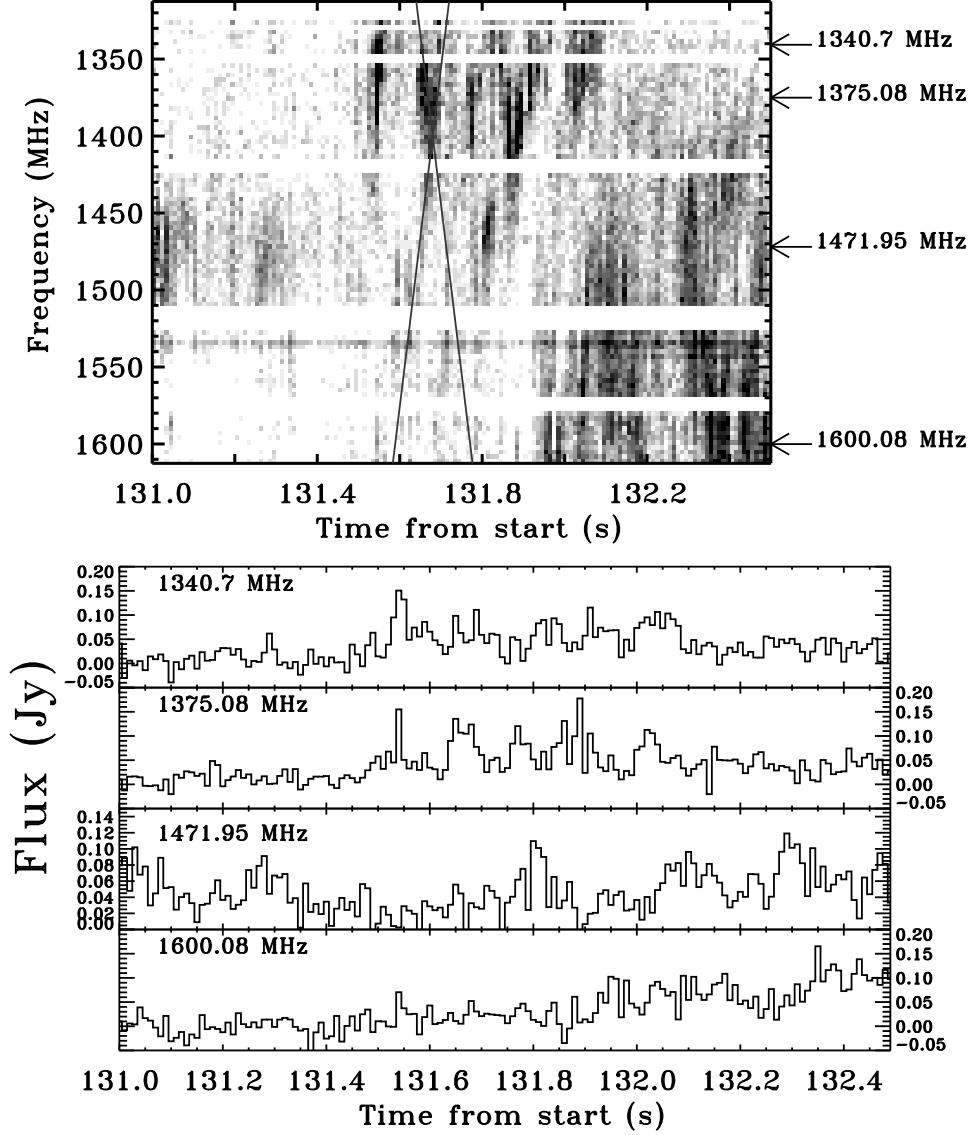
Fig. 2.— Close up of 1.5 seconds of data in event on 13 June illustrating sub-bursts with bandwidths typical of the median of the bandwidth distribution. Top panel displays portion of dynamic spectrum (300 MHz by 1.5 s), bottom panel displays light curves at four selected frequencies, noted in top panel by arrows. The black lines in the top panel indicate the characteristic drift rate of 2.2 GHz s^{-1} from a reference time and frequency point of (131.68 s, 1400 MHz), for beams directed along and in the opposite sense to the electron density gradient.
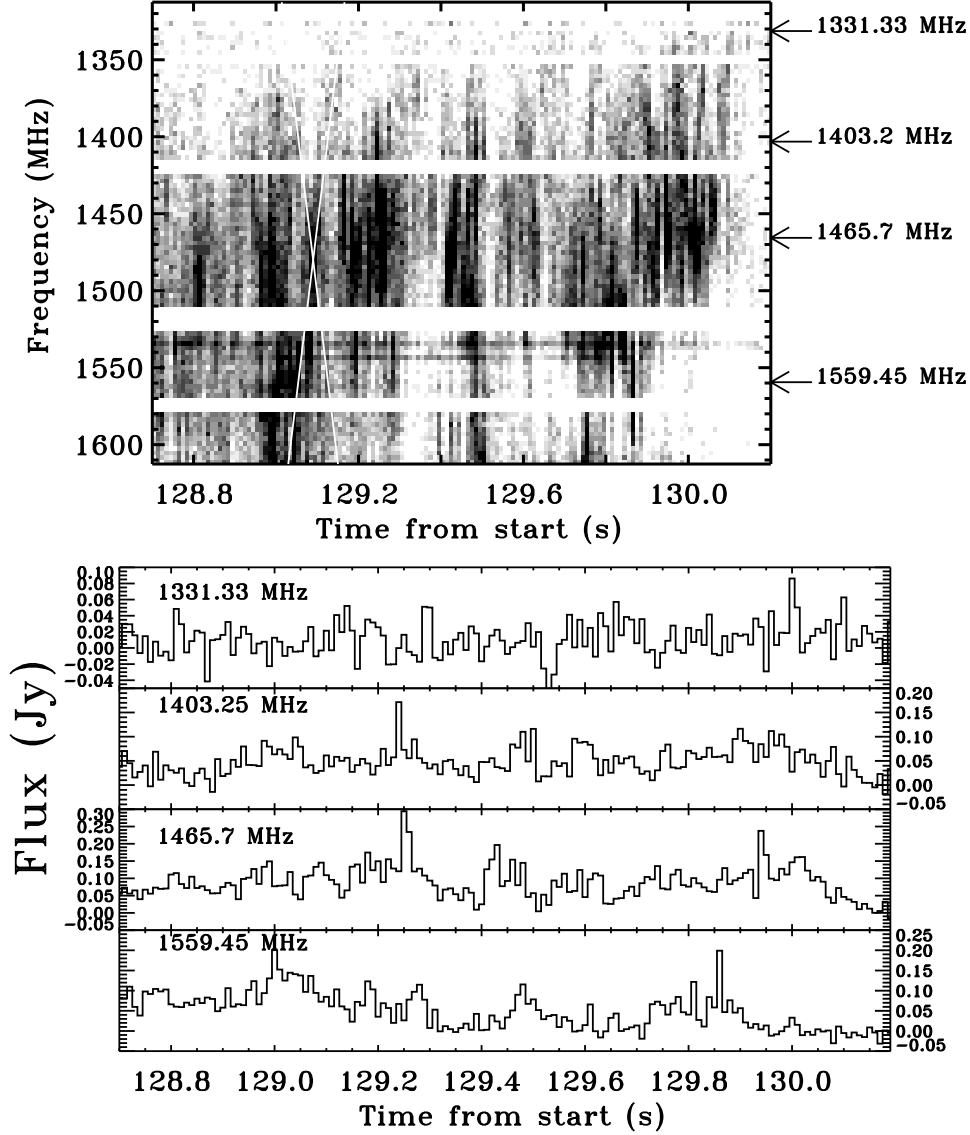
Fig. 3.— Same as for Figure 2 but for sub-bursts which occupy more frequency space. The white lines in the top panel indicate the characteristic drift rate of 2.2 GHz s^{-1} from a reference time and frequency point of (129.09 s, 1480 MHz), for beams directed along and in the opposite sense to the electron density gradient.
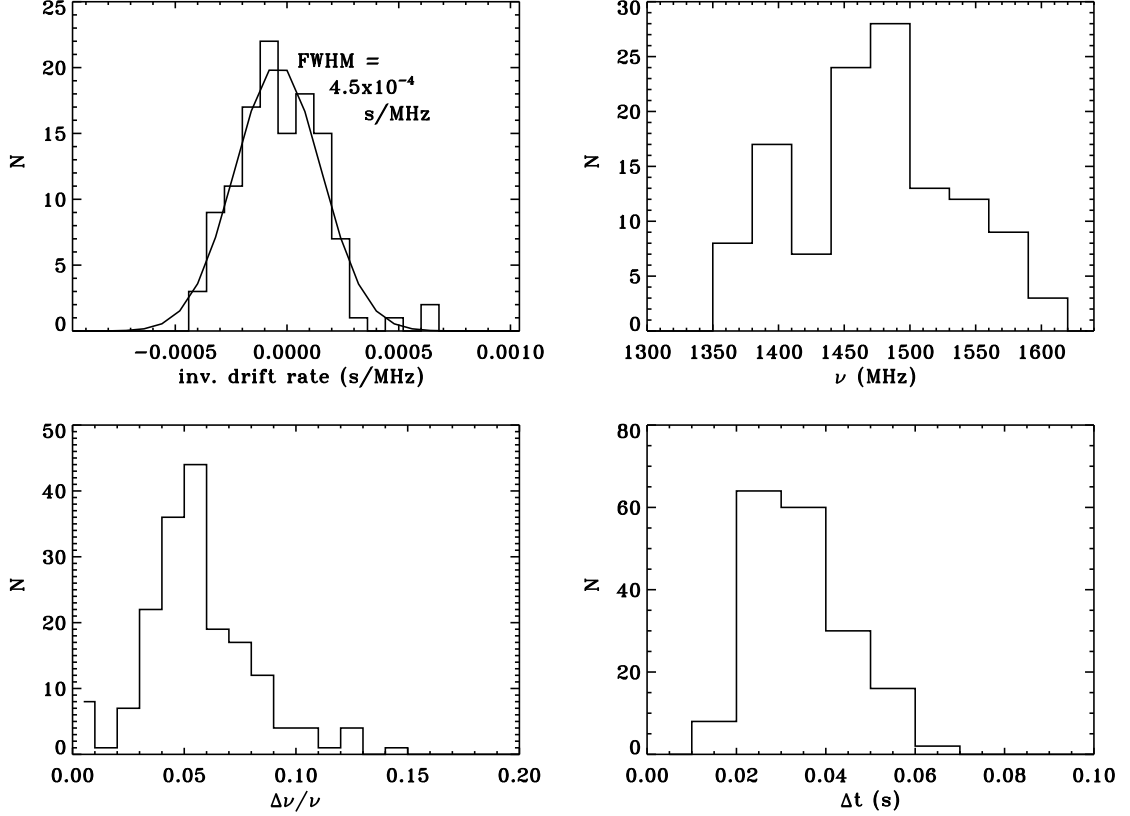
Fig. 4.— Distributions of inverse drift rates, start frequencies, bandwidths, and durations calculated for bursts seen in the 1120–1620 MHz spectral region of AD Leo, during 22:35:00–23:36:40 UT on June 13. Top left panel shows inverse drift rate distributions based on time peaks for events with nonzero duration and filtered for the flux spectrum shape (see text for details); a Gaussian fit to the distribution has a FWHM of 4.5×10^{-4} s/MHz. The top right panel displays distribution of start frequencies; this confirms that most of the sub-bursts occur at frequencies higher than $\approx$1350 MHz. Bottom left panel displays bandwidth distribution and bottom right panel display distribution of durations for events, subject to a filter; see text for details. The median bandwidth is 5% and the median duration is 0.03 s.
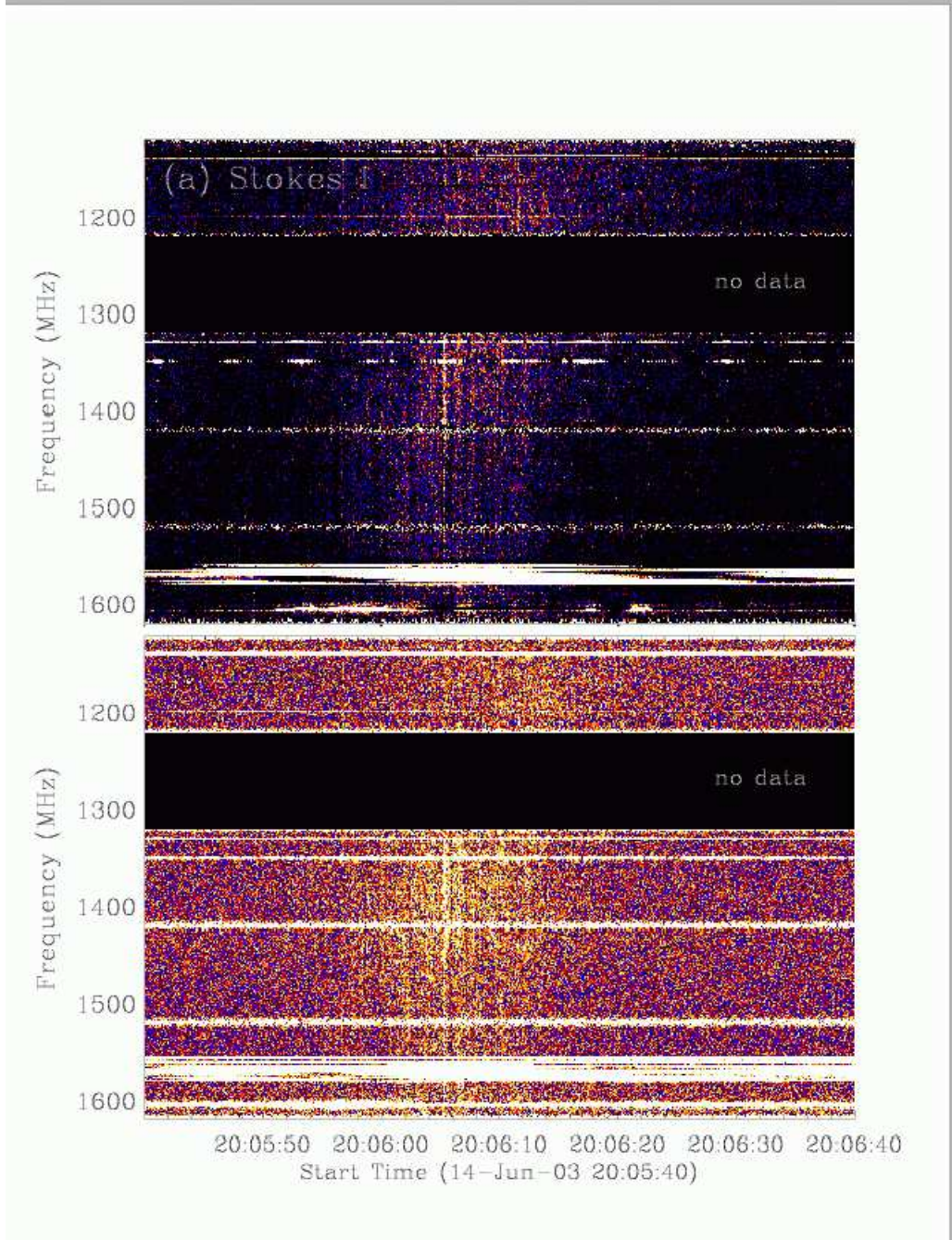
Fig. 5.— Dynamic spectrum of slowly drifting behavior seen on AD Leo with the Arecibo Observatory. Frequency increases down and time increases to the right. Frequency coverage extends from 1120–1220 MHz, 1320–1589 MHz; gaps are due to RFI excision or poor band-pass response. *(a)* Dynamic spectrum of total intensity variations. *(b)* Dynamic spectrum of circular polarization variations.
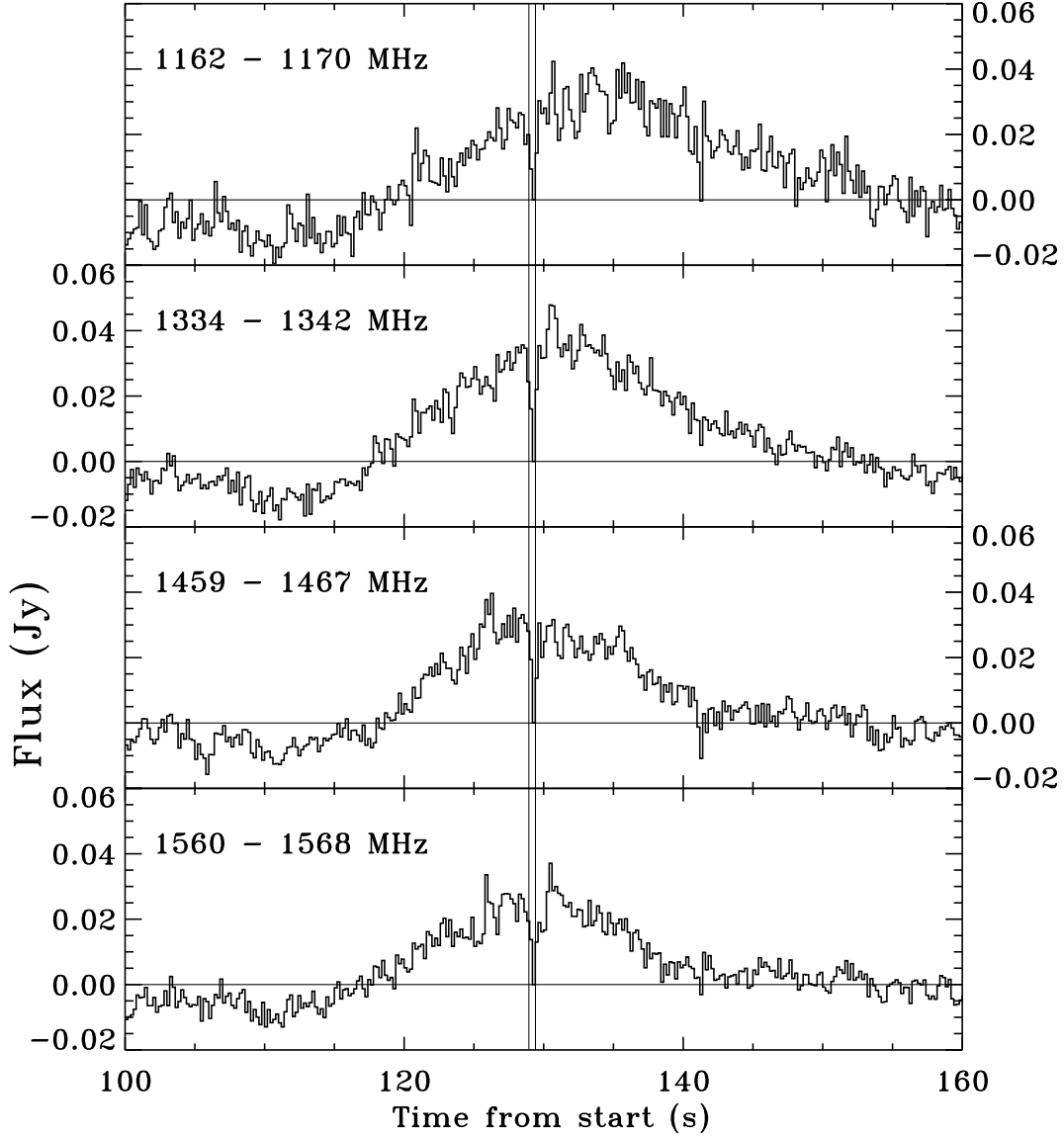
Fig. 6.— Light curves of event on June 14 at four different frequency ranges. Data have been binned by a factor of 10 in frequency and 20 in time. The data dropout at ∼129 seconds at all frequencies is due to the appearance of a periodic radar signal causing RFI; this data has been discarded. This event is characterized by a smooth, Gaussian-like modulation and the drift to lower frequencies at later times is evident.
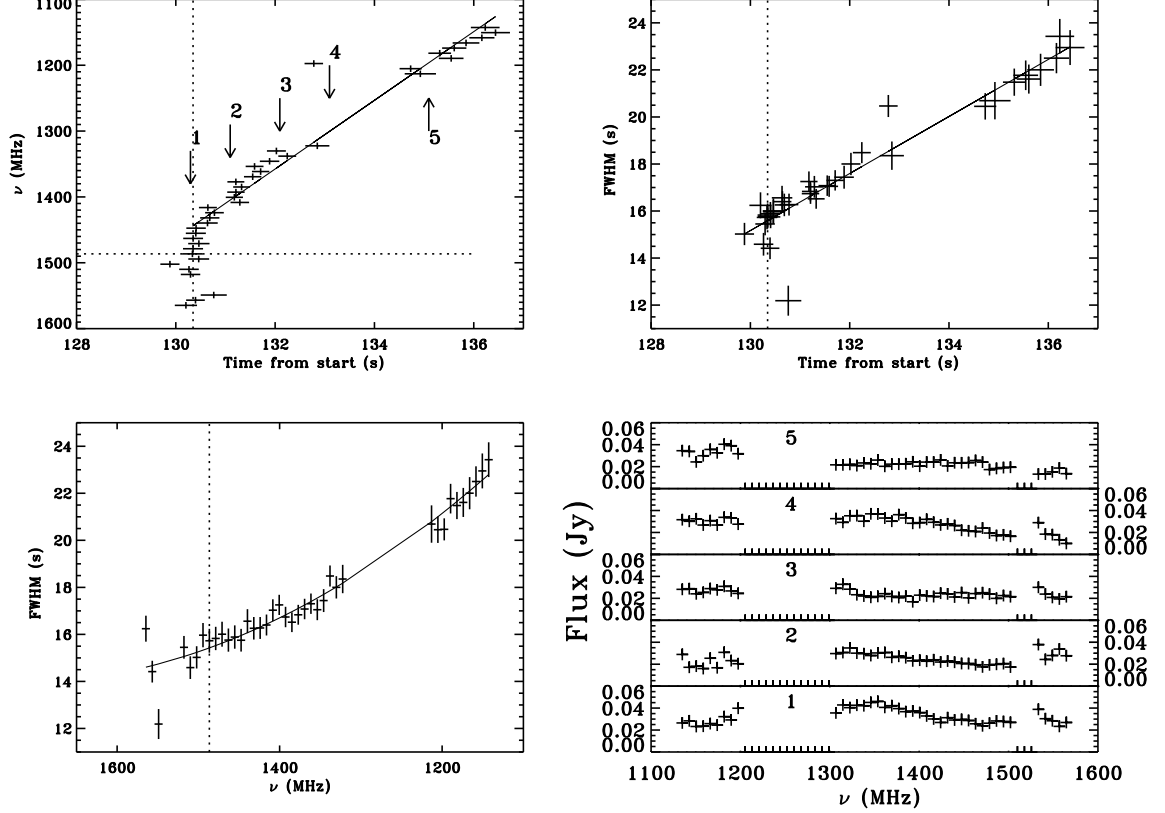
Fig. 7.— Variation of Gaussian parameters during event on 14 June 2003. Top left panel shows the central time of the Gaussian fit for each frequency bin; the linear fit to $\nu \leq 1490$ MHz is -52 MHz s^{-1}. Numbers indicate times at which flux spectra are illustrated in bottom right panel. Dashed vertical and horizontal lines indicate the approximate time and frequency, respectively, of the burst start. Top right panel shows increase of Gaussian FWHM with time; the slope of the linear fit is 1.2 FWHM (s) s^{-1}. The vertical dashed line indicates the approximate time at which the burst started, as deduced from the upper left panel. Bottom left panel displays increase of burst duration towards smaller frequencies; the solid line is a second degree polynomial fit to the data. The vertical dashed line indicates the approximate frequency at which the burst started. Bottom right panel displays the flux versus frequency at several points during the burst; numbers refer to times denoted in top left panel.